TECHNICAL PAPER

Research on vibration reduction of direct-drive piston pump based on porous variable diameter Helmholtz pulsation attenuator

Fei Gong[1] · Songlin Nie[1] · Yeqing Huang[2] · Fanglong Yin[1] · Ruidong Hong[1] · Hui Ji[1]

Abstract

Aiming at the vibration suppression and noise reduction of a direct-drive piston pump system, a novel porous variable diameter Helmholtz pulsation attenuator (abbr. PVDHPA) was developed. The vibration suppression mechanism of PVDHPA was analyzed, and the pressure and flow mathematical model was established. The fluid vibration energy absorption characteristics of PVDHPA with different structural parameters in the direct-drive pump system were analyzed by computational fluid dynamics simulation. The optimized damping hole and maximum diameter of the resonant cavity of the PVDHPA are 6.5 mm and 110 mm, respectively. Based on the custom-manufactured testing apparatus, the vibration absorption effect of the PVDHPA was verified. The test results show that the vibration response amplitude of the direct-drive pump is significantly reduced after the installation of PVDHPA, in which the vibration signals in the 200–400 Hz and 1000 Hz frequency bands are significantly suppressed, and the vibration impact in the vertical direction is most significantly weakened. Meanwhile, the foot vibration acceleration of the direct-drive pump system decreases by 7.4 dB(A). These researches provide an effective method for vibration and noise reduction of the direct-drive pump systems.

Keywords Direct-drive pump system · Helmholtz pulsation attenuator · Computational fluid dynamics · Vibration and noise

✉ Fanglong Yin
  yfl@bjut.edu.cn

  Fei Gong
  gongfei@emails.bjut.edu.cn

  Songlin Nie
  niesonglin@bjut.edu.cn

  Yeqing Huang
  huangyq29@126.com

  Ruidong Hong
  hongruidong@emails.bjut.edu.cn

  Hui Ji
  jihui@bjut.edu.cn

1 Beijing Key Laboratory of Advanced Manufacturing Technology, Beijing University of Technology, Beijing 100124, China

2 Beijing Aerospace Technology Institute, Beijing 100074, China

1 Introduction

With the development of water hydraulic technology, as the core power component of the water hydraulic systems, the application of water hydraulic pumps is becoming more and more extensive [1, 2]. Because of its high power density, high working pressure, and good reliability, the piston pump is the main structure type for the medium and high-pressure hydraulic pump [3]. The hydraulic piston pump driven by a linear motor is a new type of bilge drainage pump that sucks and drains water through the reciprocating movement of the piston. As shown in Fig. 1, the direct-drive pump system is mainly composed of eight sets of linear-drive pump units, suction pipeline, discharge pipeline, and a set of system control equipment. Each linear-drive pump unit includes a set of linear motor primary (stator) and secondary (mover), two set of pistons and cylinders, integrated cone valves, and support frame.

Compared with traditional hydraulic pump, linear-drive hydraulic pump does not require any motion conversion device, and thus, it has low vibration and high efficiency. However, when the direction of movement of the direct-drive
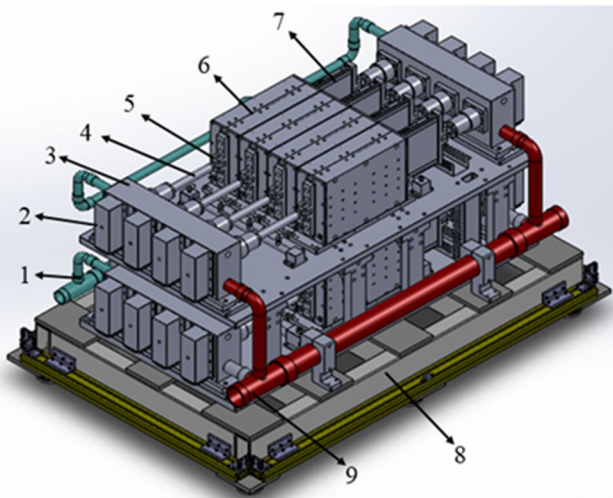
Fig. 1 Virtual prototype model of direct-drive pump system. 1-Vibration absorption pipeline, 2-Integrated Cone Valve, 3-cylinder, 4-Piston, 5-Rod end ball bearing, 6-Linear motor stator, 7-Linear motor mover, 8-Support rack, 9-Drain line

pump system changes, inertial shock is inevitable. The flow pulsation caused by the displacement mechanism of the positive displacement piston pump will form pressure pulsation after encountering the load impedance. As the fluid spread, vibration and impact will be generated on the system pipelines. These vibrations will be transmitted to the equipment body through the pipeline, which will not only reduce the concealment performance of the equipment but also affect the health status of the equipment and the living environment of the staff. Therefore, it is essential to take effective measures to mitigate the vibration level of the direct-drive pump system.

The related research work of hydraulic pump vibration and noise mainly revolves around the numerical analysis of pressure shock, flow pulsation, flow field simulation analysis, cavitation theory, and the experimental testing [4–9]. Shang et al. [10] presented a novel passive fluid ripple pulsation attenuator, which can simultaneously reduce discharge and suction pulsation of the axial-piston pump and adapt to the condition of frequent change of load reversing in closed hydraulic system. Edge et al. [11] proposed an index to evaluate the fluid noise characteristics of hydraulic pumps based on the research foundation of predecessors. In this method, the tested pump source is regarded as a parallel combination system of flow pulsation source and hydraulic pump source impedance, and the product of the two is used as the evaluation index of noise characteristics. The principle of this performance evaluation method is simple, but

it requires a long test output pipeline, which is difficult to practically use, and it is impossible to evaluate the various factors that cause pulsation individually. Additionally, Edge and Browns proposed a "Secondary source" measurement method for flow pulsation testing of hydraulic pump systems. This test method uses a laminar flow model to accurately test performance parameters such as the impedance of the tested pump source with the aid of an auxiliary pump source. The test results have high accuracy and credibility and have become an international standard for hydraulic pump fluid noise testing [12, 13]. The University of Bath has conducted a systematic research work in the field of hydraulic pump fluid noise, with remarkable results, laying a large amount of work foundation for subsequent related research. Pettersson et al. have carried out research work on the pressure and flow pulsation test of hydraulic pumps and proposed a two-point measurement method combined with the "secondary source" measurement method [14, 15]. This method uses the combination of the main pump source and volume element of the test platform to generate a wide frequency spectrum area and realizes the test of pressure and flow pulsation. In recent years, research work has been carried out on the source impedance strategy method. This method no longer establishes the mathematical model of the pump outlet pipeline, but directly measures the location of the flow pulsation source and uses the acquisition system to achieve post-processing of the test data. Manring et al. [16] carried out the numerical modeling analysis research work of piston pumps. Modeling the various stages of the piston pump working process separately makes the model more precise and detailed, but the model built by it ignores some nonlinear factors such as leakage, and the accuracy needs to be improved. Zeng and Li [17] tried to carry out numerical modeling and theoretical analysis of the pressure transient process of a piston pump with triangular damping grooves. The model ignored the influence of nonlinear factors and idealized some of the coefficients, there is greater uncertainty, and the actual application value is low.

To suppress the vibration and noise of piston pump, various hydraulic silencers have been developed. Mikota [18] proposed a method for optimizing the structure of the fluid silencer of the hydraulic system. The method is mainly to reduce the volume by combining a single-degree-of-freedom system with the cavity. By loading the "spring–mass" system, the system will achieve the same frequency as the excitation force, which will make the system anti-resonant, thereby achieving the purpose of alleviating system vibration. Orwig [19] accurately analyzed several vibration and noise measurement methods based on the noise-related spectrum analysis of the vibration emission source and the

evaluation of the most influential frequencies, providing a basis for the use of hydraulic mufflers to eliminate one or more main noise frequencies. Ijaz [20] has studied various filters and energy storage devices on rock drills and found that T-shaped tube has good adaptability to various frequencies and good pulsation attenuation effect. Ichiyanagi and Nishiumi [21] numerically evaluated the attenuation performance of the side branch resonant cavity in the hydraulic pipeline by changing parameters such as the insertion position of the side branch, the length of the connecting pipe between the side branch, and the terminal load of the circuit. Research results have shown that the degree of attenuation is determined by the insertion loss defined as the ratio of the total amplitude harmonics of the pressure pulsation with and without the side branch. Nicholas and Kenneth [22] studied the Helmholtz resonator and analyzed its performance and volume. Through the simulation and experimental analysis, the filtering effect of various parameters is obtained. Jing et al. [23] optimized the structure of the new active hydraulic silencer through previous research, simplified the structure of the product, and reduced the size of the product. Gruber et al. [24] considers the problem of finding the optimal charge pressure in either a single suppressor or two suppressors in series for maximum fluid-borne noise suppression in a weighted sense. The transmission loss, a measure of pressure ripple (dynamic pressure fluctuation) reduction, for the suppressors is predicted by an equivalent fluid model. The optimum configuration is sought through maximization of an objective function. Optimal configurations are found for a set of system pressures, load pressures, and duty cycles. It is found that the time weighting has a more significant impact on the optimum charge pressure than the frequency weighting, as seen by duty cycles considered in this paper. Yuan et al. [25] proposed acoustic energy harvester (AEH) based on an acoustic Helmholtz resonator The Helmholtz resonator was evaluated using numerical simulation and experimental tests. Experimental results illustrate that under 100 dB sound pressure level (SPL) excitation, maximum 27.2 μW power can be harvested at 217 Hz and maximum 64.4 μW power can be harvested at 341 Hz. He et al. [26] put forward a corrugated diaphragm to optimize the design of the muffler, which can absorb the pressure in the structure, thereby achieving the purpose of reducing the noise of the system.

Since the fluid excitation signal is complex and the frequency spectrum span is wide characteristics of the direct-drive pump system, the method of installing a hydraulic silencer in the connecting pipeline can obtain a more obvious and intuitive effect of vibration and noise reduction [27]. However, traditional hydraulic silencers only have

a good suppression effect on pressure pulsation within a certain frequency range, which is determined by their fixed structural rigidity. Therefore, to adapt the wide frequency range and time-varying characteristics of the direct-drive pump system, this paper proposes a new type of PVDHPA based on the Helmholtz principle. The PVDHPA effectively reduces the dynamic response of the direct-drive pump system, while being able to significantly suppress the vibration acceleration values of the machine feet. In addition, the hydraulic pump often runs under variable complexity working conditions. Therefore, it is a key issue to accurately and quickly extract the characteristic information in the vibration signal. At present, there are many methods usually used to solve the dynamic response of the system, such as discrete wavelet transform method [28, 29], Houbolt method [30], Wilson-θ method [31], and Newmark method [32]. Among them, the Newmark method has good stability and accuracy and is used as one of the oldest and most powerful methods for structural dynamic analysis and wave propagation problems. Therefore, this paper uses the Newmark method to analyze the dynamic response of the direct-drive pump with and without the installation of PVDHPA.

The structure of this paper is as follows. At first, a new PVDHPA is designed and a mathematical model, followed by the simulation of optimal structural parameters of PVDHPA. Furthermore, the vibration reduction effect of the designed PVDHPA is verified by experiments. Finally, the conclusions are drawn.
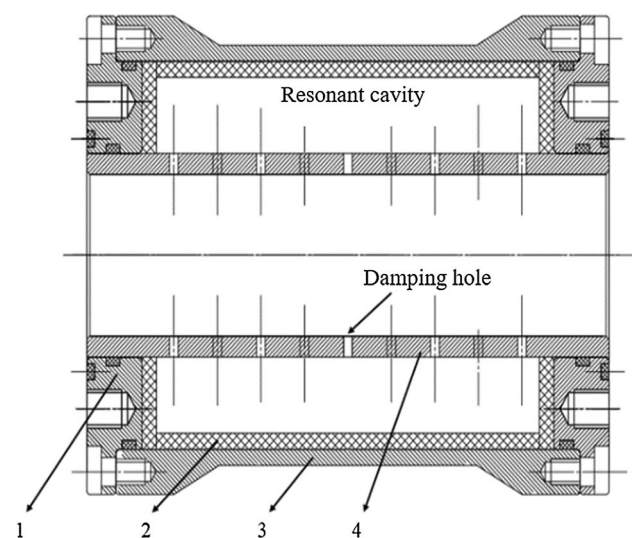

Fig. 2 Structure diagram of porous and variable diameter Helmholtz pulsation attenuator. 1-Sealed end cover, 2-Resistive vibration-absorbing material, 3-Shell, 4-Flow tube

2 Characterization, methodology, and design

2.1 Working principle

As shown in Fig. 2, the PVDHPA is mainly composed of four parts. There are multiple damping holes on the flow pipe, and each damping hole and the resonant cavity form a Helmholtz resonance unit, so the structure of the pulsation attenuator can be regarded as a series and parallel connection of multiple Helmholtz resonance units. According to the needs of the actual vibration absorption spectrum, designing multiple damping apertures of different sizes can broaden the vibration absorption frequency band and achieve a good vibration absorption effect for the high and mid-frequency bands.

As presented in Fig. 3, the working principle of the PVDHPA based on the Helmholtz principle is to use the fluid in the pipeline, the damping hole, and the resonance cavity to form a "mass–spring–damping" vibration system. The fluid in the resonance cavity is regarded as a spring, and the fluid in the damping hole is regarded as the mass, friction, and damping in the damping hole which are equivalent to the damping of the vibration system. When the frequency band of the excitation signal in the fluid is the same or close to the natural frequency of the pulsation attenuator, resonance will occur. The "fluid spring" in the damping hole has the largest amplitude and consumes a lot of energy to achieve the best filtering and damping effect.

2.2 Mathematical model

The PVDHPA structure presented in Fig. 3 is similar to a straight pipe model with branch pipelines. The differential equation of motion of a unit fluid with a length of in a straight pipe can be written as [23]:

$$\rho dx \frac{dQ}{dt} = \left[P - \left(P + \frac{\partial P}{\partial x} dx \right) \right] A_s - F_P \tag{1}$$

$$\frac{\rho}{A_s} \left(R_v Q + \frac{dQ}{dt} \right) + \frac{\partial P}{\partial x} = 0 \tag{2}$$

where ρ is the density of the fluid medium in the pipeline, A_s is the pipeline cross-sectional area, F_P is the frictional
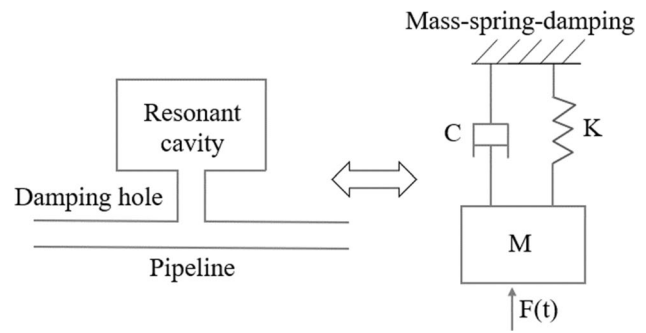

Fig. 3 Structure equivalent diagram of Helmholtz pulsation attenuator

resistance of the pipeline $F_P = R_v \rho Q dx$, and R_v is the equivalent friction coefficient.

According to the principle of flow continuity, the continuity equation of the unit fluid with length dx in the pipeline can be expressed as:

$$\frac{A_s}{K_e} \frac{\partial P}{\partial t} + \frac{\partial Q}{\partial x} = 0 \tag{3}$$

where K_e is the apparent bulk modulus, which can be calculated by $\frac{1}{K_e} = \frac{1}{K} + \frac{1}{K_p}$, K_p is the elastic modulus of pipeline and $K_p = \frac{\delta E}{d}$, d is the inner diameter of pipeline, E is the elastic modulus of pipeline material, and K is the bulk elastic modulus of the fluid medium. The Laplace transform of Eqs. (2) and (3) are given as:

$$\begin{cases} \frac{\rho}{A_s} (R_v + s) Q(s) + \frac{\partial P(s)}{\partial x} = 0 \\ \frac{A_s}{K_e} s P(s) + \frac{\partial Q(s)}{\partial x} = 0 \end{cases} \tag{4}$$

It can be obtained by simplifying Eq. (4)

$$\frac{\partial^2 P(s)}{\partial^2 x} - \frac{\rho(s^2 + R_v s)}{K_e} P(s) = 0 \tag{5}$$

The general solution of Eq. (5) is:

$$P(s) = C_1 ch\left(\sqrt{\frac{\rho(s^2 + R_v s)}{K_e}} x \right) + C_2 sh\left(\sqrt{\frac{\rho(s^2 + R_v s)}{K_e}} x \right) \tag{6}$$

The same can be obtained:

$$Q(s) = -\frac{A_s}{\sqrt{\rho\left(1 + \frac{R_v}{s}\right)}} \left[C_1 sh\left(\sqrt{\frac{\rho(s^2 + R_v s)}{K_e}} x \right) + C_2 ch\left(\sqrt{\frac{\rho(s^2 + R_v s)}{K_e}} x \right) \right] \tag{7}$$

Based on Eqs. (6) and (7), the input, output pressure, and flow state equations in the straight pipe section of length L are processed based on the distributed parameters:

$$\begin{bmatrix} P_i(s) \\ Q_i(s) \end{bmatrix} = T_i \begin{bmatrix} 1 & 0 \\ \frac{1}{Z_3(s)} + \cdots + \frac{1}{Z_{n+2}(s)} & 1 \end{bmatrix} T_o \begin{bmatrix} P_o(s) \\ Q_o(s) \end{bmatrix} \quad (14)$$

$$\begin{cases} P_i(s) = P_o(s)ch\left(\sqrt{\frac{\rho(s^2 + R_\upsilon s)}{K_e}}L\right) - Q_o(s)\frac{\sqrt{\rho K_e(s^2 + R_\upsilon s)}}{A_s s}sh\left(\sqrt{\frac{\rho(s^2 + R_\upsilon s)}{K_e}}L\right) \\ \\ Q_i(s) = -P_o(s)\frac{A_s s}{\sqrt{\rho K_e(s^2 + R_\upsilon s)}}sh\left(\sqrt{\frac{\rho(s^2 + R_\upsilon s)}{K_e}}L\right) + Q_o(s)ch\left(\sqrt{\frac{\rho(s^2 + R_\upsilon s)}{K_e}}L\right) \end{cases} \quad (8)$$

Let $\tau(s) = \sqrt{\frac{\rho(s^2 + R_\upsilon s)}{K_e}}$, $Z(s) = \frac{\sqrt{\rho K_e(s^2 + R_\upsilon s)}}{A_s s}$, then Eq. (8) can be presented as:

$$\begin{bmatrix} P_i(s) \\ Q_i(s) \end{bmatrix} = \begin{bmatrix} ch[\tau(s)L] & -Z(s)sh[\tau(s)L] \\ -\frac{1}{Z(s)}sh[\tau(s)L] & ch[\tau(s)L] \end{bmatrix} \begin{bmatrix} P_o(s) \\ Q_o(s) \end{bmatrix} \quad (9)$$

where

$$T = \begin{bmatrix} ch[\tau(s)L] & -Z(s)sh[\tau(s)L] \\ -\frac{1}{Z(s)}sh[\tau(s)L] & ch[\tau(s)L] \end{bmatrix}$$

At the branch pipeline, supposing the pressure and flow in the inlet pipeline, outlet pipeline, and branch damping hole are, respectively, (P_1, Q_1), (P_2, Q_2), (P_3, Q_3), the pressure and flow model can be expressed as:

$$\begin{cases} P_1 = P_2 = P_3 \\ Q_1 = Q_2 + Q_3 \end{cases} \quad (10)$$

P_3 is given as

$$P_3 = Q_3 \cdot Z_3 \quad (11)$$

Combining Eqs. (10) and (11), the pressure and flow model can be obtained by

$$\begin{bmatrix} P_1(s) \\ Q_1(s) \end{bmatrix} = \begin{bmatrix} 1 & 0 \\ \frac{1}{Z_3(s)} & 1 \end{bmatrix} \begin{bmatrix} P_2(s) \\ Q_2(s) \end{bmatrix} \quad (12)$$

For a pipeline with multiple continuous branch damping holes, it can be represented as:

$$\begin{bmatrix} P_1(s) \\ Q_1(s) \end{bmatrix} = \begin{bmatrix} 1 & 0 \\ \frac{1}{Z_3(s)} + \cdots + \frac{1}{Z_{n+2}(s)} & 1 \end{bmatrix} \begin{bmatrix} P_2(s) \\ Q_2(s) \end{bmatrix} \quad (13)$$

Combining the mathematical models of Eqs. (9) and (13), the pressure and flow mathematical model of the porous reduced-diameter Helmholtz pulsation attenuator used in this system can be defined:

where T_i and T_o are transfer matrix of inlet straight pipe section and outlet straight pipe section, respectively.

2.3 Sensitivity analysis of structural parameters

Based on the mathematical analytical model constructed in the previous chapter, the fluid simulation method is used to analyze the absorption characteristics of the fluid vibration energy of the direct-drive pump system with different structural parameters of the PVDHPA.

Based on the working principle of Helmholtz resonant cavity, its resonant frequency is defined as

$$f_h = \frac{c_0 d_h}{4\sqrt{LV_h\pi}} \quad (15)$$

where c_0 is the speed of sound in the fluid, d_h is the diameter of the damping hole, L is the length of the damping hole, and V_h is the volume of the resonant cavity.

After the Helmholtz pulsation attenuator, the transmission loss of fluid vibration energy can be calculated as

$$TL = 10\lg\left[1 + \left(\frac{\frac{\sqrt{S_c V_h / L}}{2S_m}}{\frac{f_h}{f_r} - \frac{f_r}{f_h}}\right)^2\right] \quad (16)$$

where S_c is the cross-sectional area of damping hole, S_m is the section area of the main pipeline, and f_r is the exciting frequency.

It can be seen from the above mathematical model that the main variable structural parameters that affect the vibration absorption characteristics of the PVDHPA include the length of the damping hole, the size of the aperture, and the volume of the resonant cavity when the excitation signal and working conditions are determined. Using the flow field simulation analysis method, the distribution characteristics of the pressure, flow, velocity, turbulent energy, and other physical quantities in the fluid domain can be obtained to
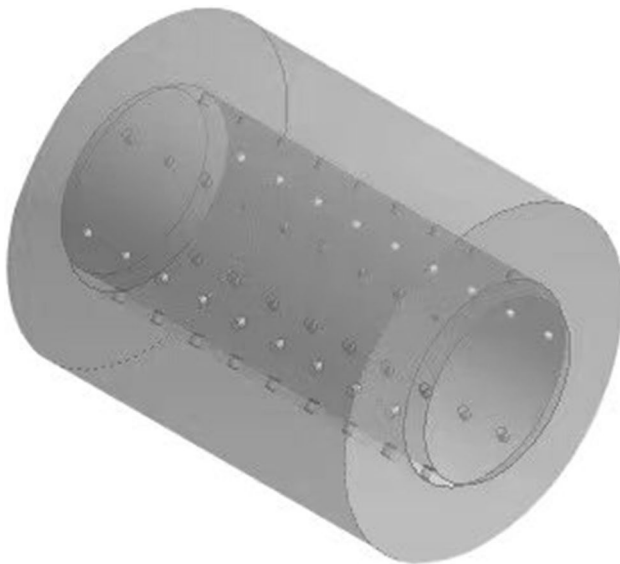
Fig. 4 Fluid domain model of Helmholtz pulsation attenuator

Table 1 Parameters for CFD simulation

Description	Value
Fluid density (kg/m^3)	1×10^3
Fluid dynamic viscosity (Pa s)	1.01×10^{-3}
Diameter of the damping hole (mm)	3.0
Length of the damping hole (mm)	3.0, 4.0, 5.0, 6.5
Resonant cavity maximum diameter (mm)	110.0
Working pressure of the pump (MPa)	4.0
Flow rate of the pump (L/min)	330.0
Wall	Stationary

Fig. 5 Velocity contour under rated condition
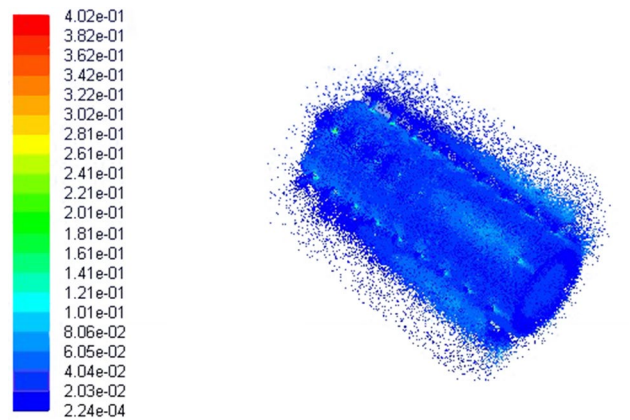
Fig. 6 Turbulent kinetic energy contour under rated condition

study the sensitivity of the flow field characteristics to different structural parameters.

Considering the actual application conditions of the PVDHPA, the dynamic energy dissipation of the fluid is obvious under the action of the resonance unit formed by the damping hole and the resonant cavity, so the realizable k–ε turbulence model is used for simulation calculation. The realizable k–ε turbulence model is used to describe the state of the flow field in the pulsation attenuator, and the governing equations of its turbulent kinetic energy and turbulent energy dissipation rate are expressed as:

$$\frac{\partial(\rho k)}{\partial t} + \frac{\partial(\rho k u_i)}{\partial x_i} = \frac{\partial}{\partial x_j}\left[\left(\mu + \frac{\mu_t}{\sigma_k}\right)\frac{\partial k}{\partial x_j}\right] + G_k + G_b - \rho\varepsilon - Y_M \tag{17}$$
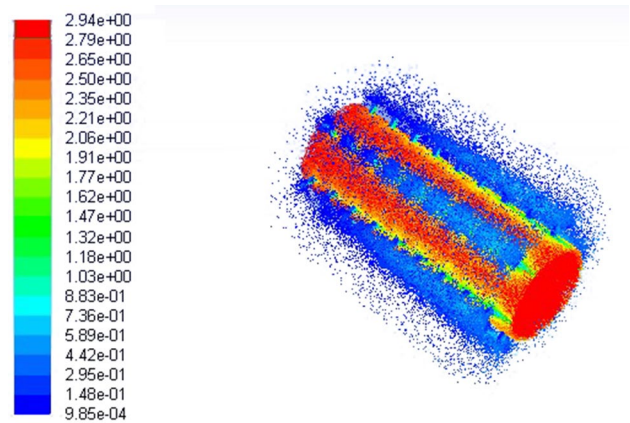
$$\frac{\partial(\rho\varepsilon)}{\partial t} + \frac{\partial(\rho\varepsilon u_i)}{\partial x_i} = \frac{\partial}{\partial x_j}\left[\left(\mu + \frac{\mu_t}{\sigma_\varepsilon}\right)\frac{\partial\varepsilon}{\partial x_j}\right] + \rho C_1 E\varepsilon - \rho C_2 \frac{\varepsilon^2}{k + \sqrt{\upsilon\varepsilon}} + C_{1\varepsilon}\frac{\varepsilon}{k}C_{3\varepsilon}G_b \tag{18}$$

where ρ is the density of the fluid medium, k is the turbulent kinetic energy, ε is the turbulent energy dissipation rate, G_k is the turbulent kinetic energy component produced by the average velocity gradient, G_b is the turbulent kinetic energy component produced by the influence of buoyancy, Y_M is the effect of compressible turbulent arterial expansion on the total kinetic energy dissipation rate, σ_k and σ_ε are turbulent Prandtl number of turbulent kinetic energy and turbulent energy dissipation rate, respectively, and μ is the molecular viscosity coefficient.

As shown in Fig. 4, a three-dimensional fluid domain model of the PVDHPA was established using the Solidworks 3D graphics software and importing into ANSYS fluent, and the MultiZone method was used for mesh division to generate a hexahedral mesh. During the simulation process, the fluid material is set according to the properties of pure water, and the main CFD simulation parameters are listed in Table 1. Additionally, the assumptions and limitations of the proposed method are as follows:

1. A constant stable pure water supply is considered.
2. The entering fluid is incompressible, and the fluid flow is set to laminar.
3. Flowing process of pure water through of PVDHPA is isentropic.
4. Dynamic flow forces, pure water inertia, and pressure loss in tubes are neglected.
5. The erosion effects due to cavitation have not been taken into account.

The velocity contour and turbulence kinetic energy contour of the PVDHPA can be intuitively observed in Figs. 5 and 6, respectively. In a resonant cavity connected in parallel with multiple damping holes, the flow velocity is low, indicating that there is a less fluid medium exchange in the cavity, and the fluid in the cavity exists as a spring in the equivalent resonance model; taking the resonant cavity as the dividing line, the flow velocity in the damping hole begins to increase, and the motion state becomes active. The fluid in the damping hole exists in the form of a mass in the equivalent resonance model, which is under the combined action of the main pipe fluid, the resonance chamber fluid, and the friction force of the damping hole sports. It can be found in Fig. 6 that turbulent kinetic energy fluctuates significantly in the fluid domain near the damping hole. The maximum value of turbulent kinetic energy and turbulent energy dissipation rate is concentrated near the damping hole, indicating the excitation energy in the fluid medium. Under the action of the damping hole and the resonant cavity structure, a large degree of dissipation is obtained. Under the same working conditions and fluid excitation signal source, the larger the value of the turbulent energy dissipation rate, the better the vibration absorption effect of the corresponding shock-absorber structure. Therefore, in the simulation
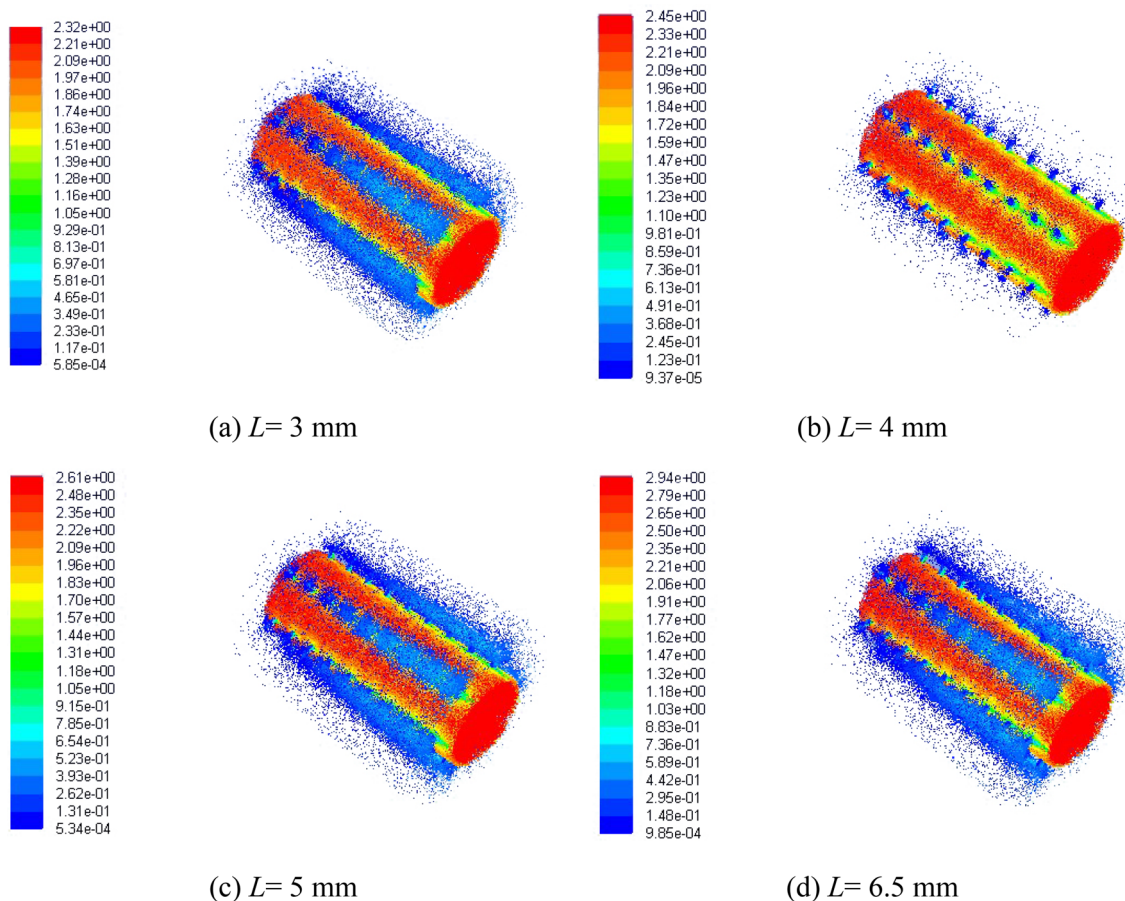

(a) L= 3 mm

(b) L= 4 mm

(c) L= 5 mm

(d) L= 6.5 mm

Fig. 7 Flow field velocity characteristic vector contour of different damping hole lengths
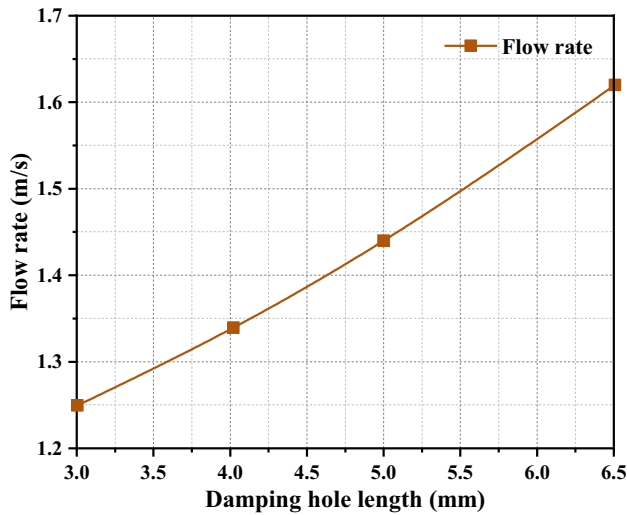
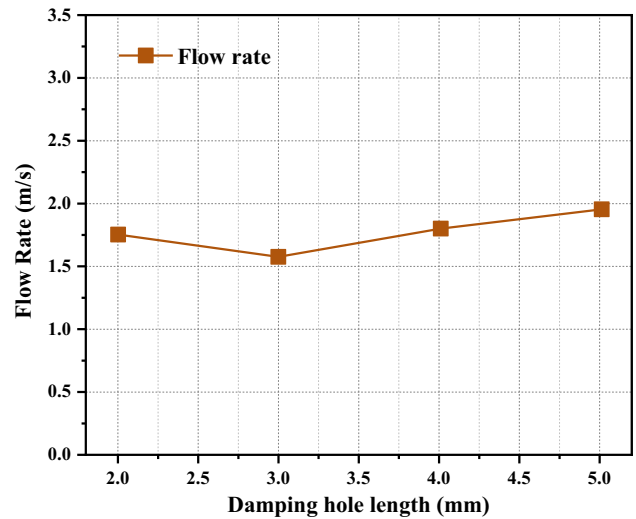**Fig. 8** Flow velocity in the damping hole varying with the length of the damping hole

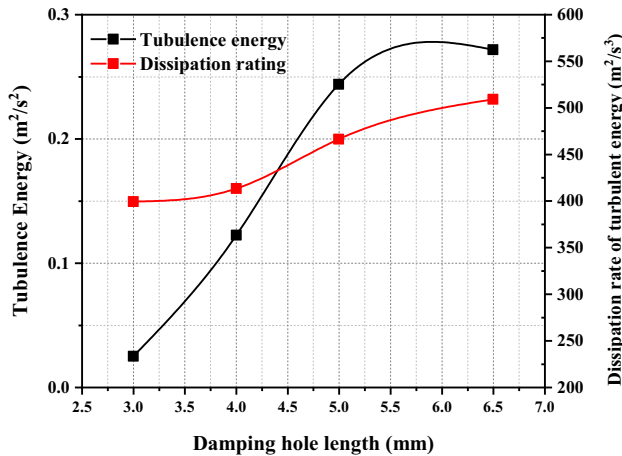**Fig. 10** Flow velocity in the damping hole varying with the diameter of the damping hole

Fig. 9 Turbulent kinetic energy and dissipation rate in the damping hole varying with the length of the damping hole
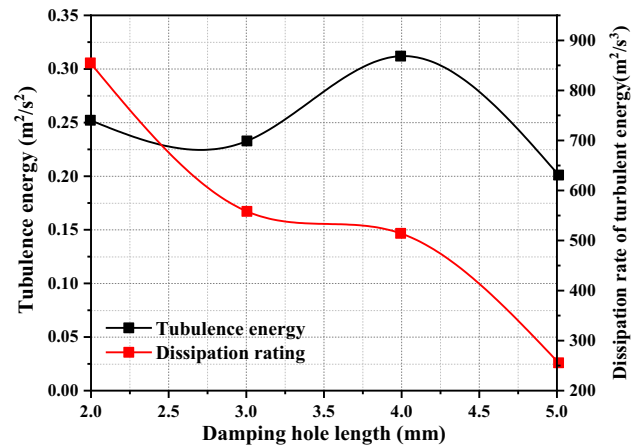

Fig. 11 Turbulent kinetic energy and dissipation rate in the damping hole varying with the diameter of the damping hole

analysis of the flow field of the PVDHPA, the flow velocity, turbulent flow energy, and turbulent dissipation rate in the damping hole can be used as a reference index for its vibration absorption performance.

The damping hole lengths have significant impacts on the operational performance of the PVDHPA. It not only increases the medium flow velocity but also leads to turbulent kinetic energy, both of which contribute to a higher turbulent energy dissipation rate. Figure 7 shows the flow velocity of the resonant cavity under different damping hole lengths. The effect of different damping hole lengths on the flow field characteristic is carried out with the damping hole diameter of 3 mm and the maximum resonant cavity diameter of 110 mm. The flow velocity in the damping hole is

mainly influenced by the pressure difference on both sides of the outlet pipeline and the resonance cavity. The increase in damping hole length could increase the pressure difference between the two sides of the damping hole, resulting in a linear increase in the flow velocity.

In order to quantitatively describe the characteristics of the flow field velocity. The velocity, turbulent kinetic energy, and turbulent kinetic energy dissipation rate of the fluid domain in the damping hole were plotted as a function of the length of the damping hole. As shown in Figs. 8 and 9, the working conditions of the direct-drive pump system and the fluid excitation signal source are determined, and other structural parameters are not changed. As the length of the damping hole increases, the flow velocity, turbulent kinetic
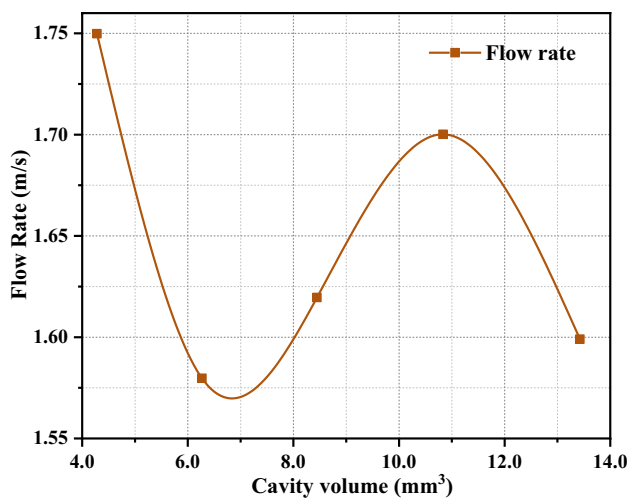
Fig. 12 Flow velocity in the damping hole varying with the resonant cavity volume
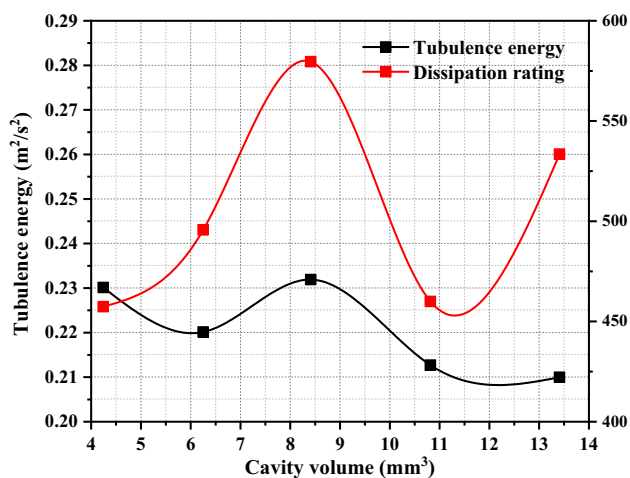

Fig. 13 Turbulent kinetic energy and dissipation rate in the damping hole varying with the resonant cavity volume

energy, and turbulent energy dissipation rate also gradually increase. The fluid flow rate and the length of the damping hole are linear; the increase in the turbulent energy dissipation rate parameter value is more obvious when the length of the damping hole is less than 5 mm, and the increase begins to decrease after the length of the damping hole exceeds 5 mm. When designing the structural parameters of the pulsation attenuator, the length of the damping hole should be appropriately increased within the allowable range of the overall structure, which can increase the turbulent energy dissipation rate and enhance the Helmholtz pulsation attenuator ability to absorb the excitation energy in the fluid.

Under the structural parameters that the length of the damping hole is 6.5 mm and the maximum diameter of the resonant cavity is 110 mm, the flow field analysis of

different damping hole diameter parameters is carried out, respectively, and the velocity, turbulent kinetic energy, and turbulent energy dissipation rate of the fluid domain in the damping hole are obtained. It is illustrated in Figs. 10 and 11 that when the working conditions of the direct-drive pump system and the fluid excitation signal source are determined, other structural parameters are not changed. As the diameter of the damping hole increases, the flow rate first decreases and then increases, and the minimum value of the flow rate is near 3 mm of the damping hole length. The turbulent energy dissipation rate gradually decreases with the increase in the damping hole diameter; when the damping hole diameter is 2 mm, the turbulent energy dissipation rate reaches 857, and there is a platform area near 3–4 mm, and the damping hole diameter is 5 mm When the turbulent energy dissipation rate was only 256, it was reduced by 70%. From the perspective of enhancing the vibration absorbing performance of the PVDHPA, and considering the flow rate of the main pipeline under the rated working conditions, the diameter of the damping hole should be appropriately reduced to help improve the overall vibration damping effect.

Under the damping hole with a diameter of 3 mm and a length of 6.5 mm, the flow field analysis of different cavity volume parameters is carried out, and the velocity, turbulent kinetic energy, and turbulent energy dissipation rate of the fluid domain in the damping hole varying with the volume of the cavity are shown in Figs. 12 and 13. To facilitate the model design and flow field characteristic parameter analysis, the maximum diameter of the resonant cavity is used as the independent variable of the volume change of the resonant cavity. As can be seen in Figs. 12 and 13, when the working conditions of the direct-drive pump system and the fluid excitation signal source are determined, other structural parameters, such as fluid flow rate, turbulent kinetic energy, and turbulent energy dissipation rate, are not changed. As the volume of the resonant cavity increases, it fluctuates in a wave shape. When the maximum diameter of the cavity is 110 mm, the maximum value of the turbulent energy dissipation rate is 562; when the maximum diameter of the cavity is 120 mm, the maximum value of the turbulent energy dissipation rate is at the minimum point, about 452. Appropriately increasing the volume of the resonant cavity will achieve a relatively good vibration damping effect, but due to the overall structural size of the PVDHPA and the piping arrangement, it is necessary to select the relative maximum point of the turbulent dissipation rate according to the actual working conditions.

According to the results obtained from the analysis of the characteristics of the throttling field and the optimization design calculation of the main structural parameters, the length of the damping hole is selected as 6.5 mm, the maximum diameter of the resonant cavity is 110 mm, and

Fig. 14 Schematic diagram of the PVDHPA test system

Fig. 15 Prototype of PVDHPA and schematic diagram of vibration test point arrangement
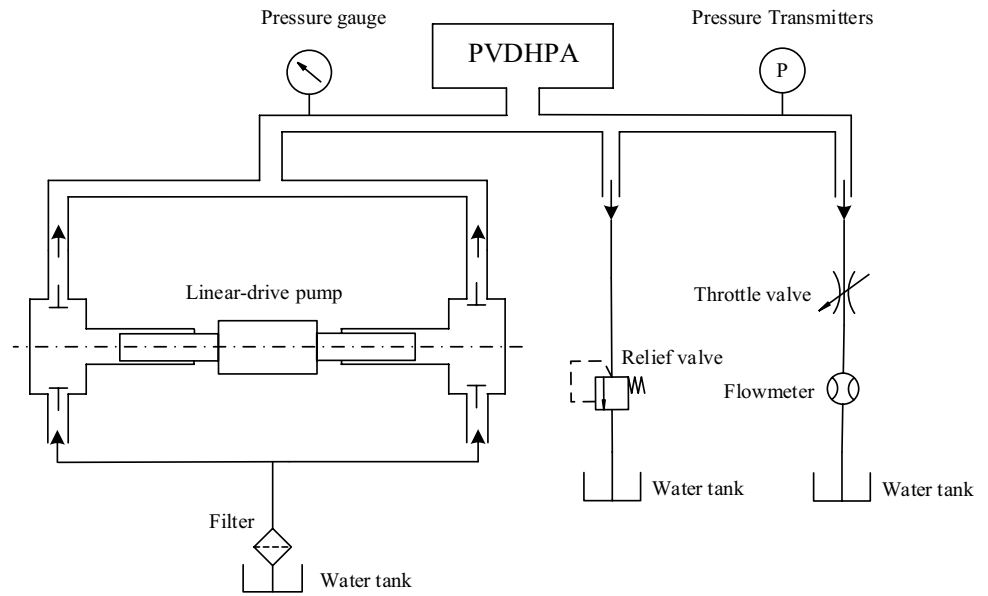
the diameter of the damping hole is in the range of 2–4 mm. The structure of a variable-diameter damping hole is used to broaden the resonance frequency band of the pulsation attenuator and use the mechanical structure to optimize the vibration and noise reduction of the direct-drive pump system.

3 Experimental study

3.1 Performance test method

From the numerical results obtained, the optimal structural parameters of the pulsation attenuator prototype are determined. The resistive vibration absorbing material is nylon. Figures 14 and 15 present the schematic diagram and practicality picture of the PVDHPA test system, respectively. A multi-channel vibration test acquisition analyzer was used to carry out the vibration signal test experiment of the direct-drive pump system. To ensure the accuracy of the vibration test results and minimize the measurement error, three data collection points were symmetrically arranged on the bottom support platform of the direct-drive pump system.

Each test point was sampled three times, and the average value was taken to complete the analysis of the intensity and the vibration acceleration value of the machine foot. The probe of the vibration signal acquisition instrument can collect the vibration acceleration of each test point in the three directions of X, Y, and Z in the space. The X-horizontal plane is perpendicular to the linear motor movement direction, Y-the linear motor movement direction, Z-vertical direction.

The sampled vibration acceleration signal is processed by the vibration test analysis software platform Coinv Dasp10 to obtain the vibration velocity of the sampling test point in different directions in X, Y, Z and calculate the vibration intensity value of the direct-drive pump. Based on the national standards for vibration intensity testing and evaluation, the root-mean-square value of the vibration velocity is defined as a measurement scale that characterizes the vibration intensity of the system, as shown in Eq. (19).

$$V_{\mathrm{rms}} = \sqrt{\frac{1}{T} \int_0^T v^2(t)\mathrm{d}t} \tag{19}$$

where V_{rms} is the root-mean-square value of vibration velocity, $v(t)$ is the vibration speed as a function of time, and T is the measuring period.

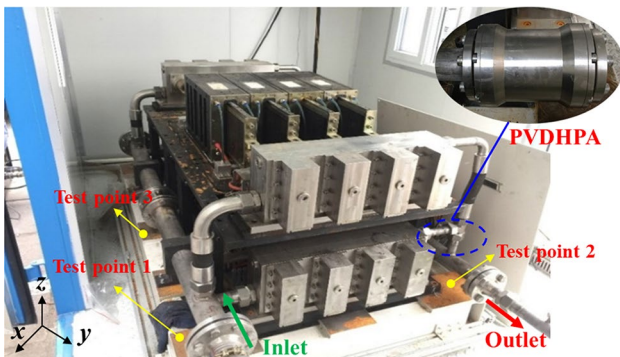The definition expression of vibration intensity can be written as:

(a) Without PVDHPA
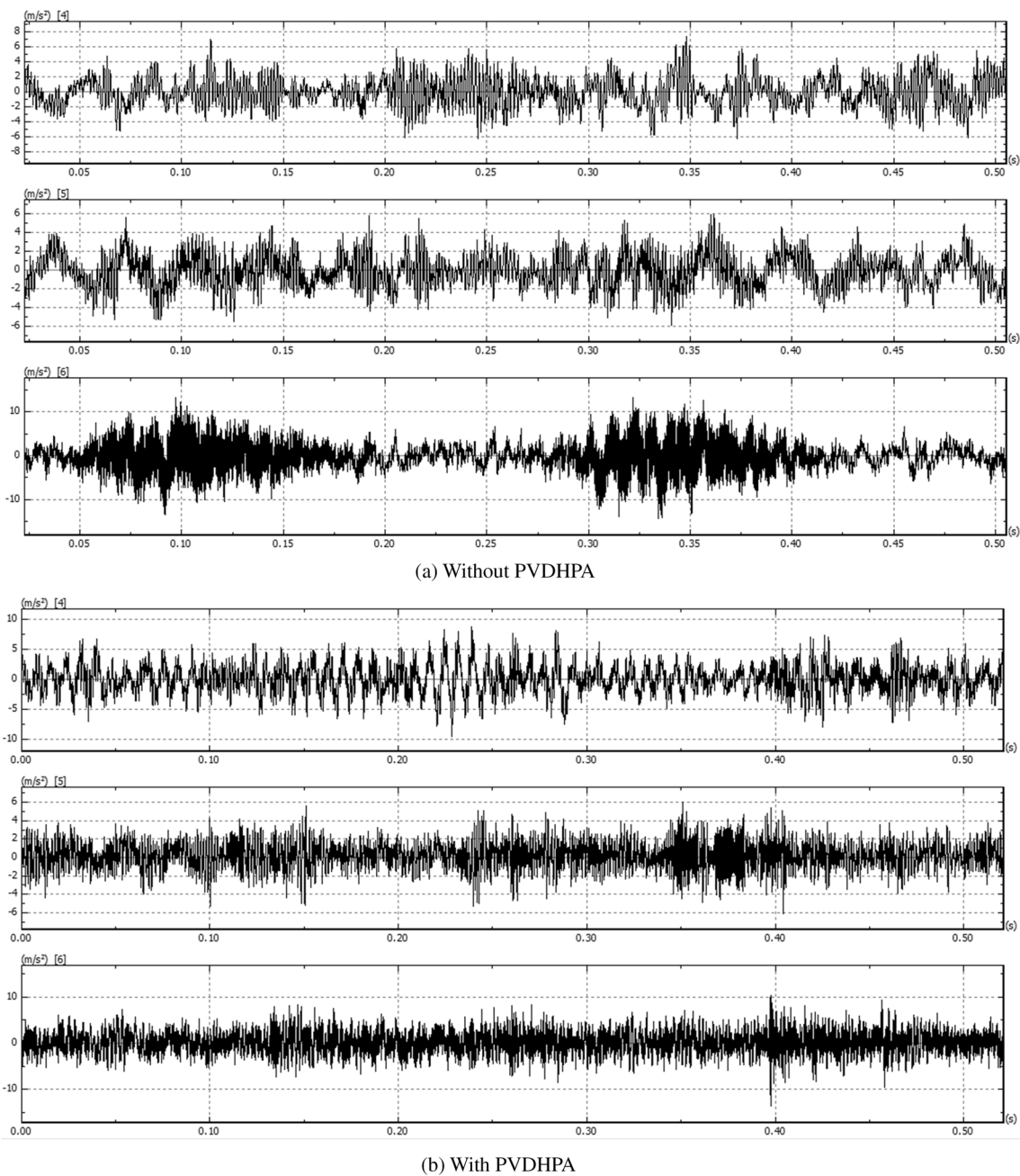

(b) With PVDHPA

Fig. 16 Time-domain signal of vibration acceleration without and with the installation of PVDHPA

$$V_s = \sqrt{\left(\frac{\sum V_x}{N_x}\right)^2 + \left(\frac{\sum V_y}{N_y}\right)^2 + \left(\frac{\sum V_z}{N_z}\right)^2} \qquad (20)$$

where V_s is the vibration intensity, V_x, V_y, and V_z are the root-mean-square value of vibration velocity in X, Y, and Z directions, respectively, and N_x, N_y, and N_z are the several test points in X, Y, and Z directions, respectively.

3.2 Performance test results and analysis

To analyze the actual vibration reduction effect of the proposed PVDHPA under working pressure of 4 MPa and flow rate of 330 L/min, the Newmark time integration method is used to measure the vibration acceleration responses of the X-, Y-, and Z-axes, as shown in Fig. 16. As can be seen from Fig. 16, the vibration and shock signal of the direct-drive
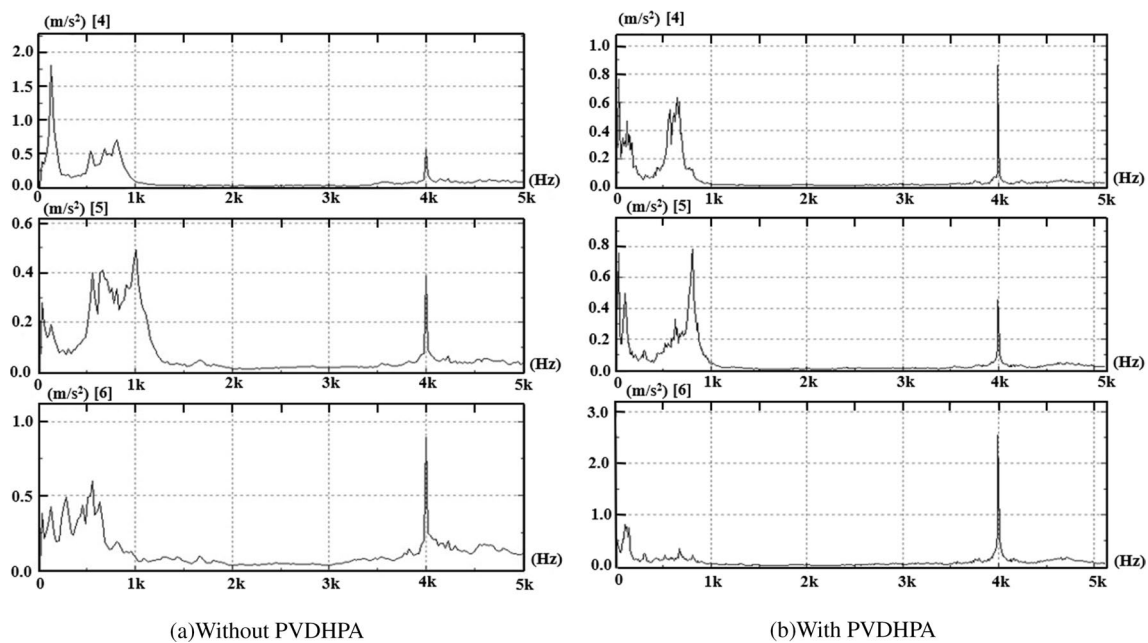
Fig. 17 Frequency-domain signal of vibration acceleration without and with the installation of PVDHPA

Table 2 Vibration severity under different working pressures (Unit: mm/s)

Experimental condition	0 MPa	1 MPa	2 MPa	3 MPa	4 MPa
With the PVDHPA	3.5	3.7	3.9	4.3	4.4
Without the PVDHPA	7.0	7.1	7.9	8.9	10.2

pump system has periodic changes, which are the same as the reciprocating cycle of the linear motor, indicating that the pressure and flow shock caused by the continuous reciprocating movement of the linear motor are the main causes of system vibration factor. Comparing the time-domain signal curve of vibration acceleration before and after the installation of the Helmholtz pulsation attenuator, it can be found that the amplitude of the vibration signal is significantly weakened after the installation of the pulsation attenuator, and the vibration acceleration waveform curve is more stable.

Figure 17 illustrates the collected vibration acceleration signal curve in frequency domain. It is clear that before the PVDHPA is installed, the extreme values of the vibration signal spectrum are mainly distributed in several frequency ranges around 100 Hz, 200 Hz, 400 Hz, 600 Hz, and 4000 Hz. A wide range of excitation signals excites the direct-drive pump system components to resonate. Comparing the analysis results of the structural mechanical characteristics of the direct-drive pump system in Sect. 3.2, the low-order natural frequency of the system is distributed between 63 and 345 Hz, which is the same as the resonance

frequency range obtained by the actual vibration test analysis.

Comparing and analyzing the frequency-domain curve of the vibration acceleration signal before and after the installation of the PVDHPA, it can be found that after the vibration signal in the frequency range around 200–400 Hz and 1000 Hz is significantly suppressed by the PVDHPA, the vibration shock in the vertical direction is weakened. Most obviously, the high-frequency vibration signal changes little. The test results show that the designed PVDHPA based on the dynamic characteristics analysis has a good filtering effect on the excitation signal in the frequency range of 200–400 Hz. Moreover, it has a better absorption effect on the vibration signal near 1000 Hz and high frequency. Consequently, the actual test results are consistent with the design analysis, verifying the correctness of the model and simulation analysis of the PVDHPA.

4 Results and discussion

The use of pipeline pulsation attenuator to weaken the resonance of the excitation signal and the main components could reduce the overall vibration amplitude of the direct-drive pump system. The Newmark method is applied to the collected vibration acceleration signals taken to solve the dynamic response of the vibration system in the three directions of X, Y, and Z in space. The strength and vibration acceleration of the direct-drive pump system can be obtained by Eqs. (19) and (20). Table 2 lists the vibration
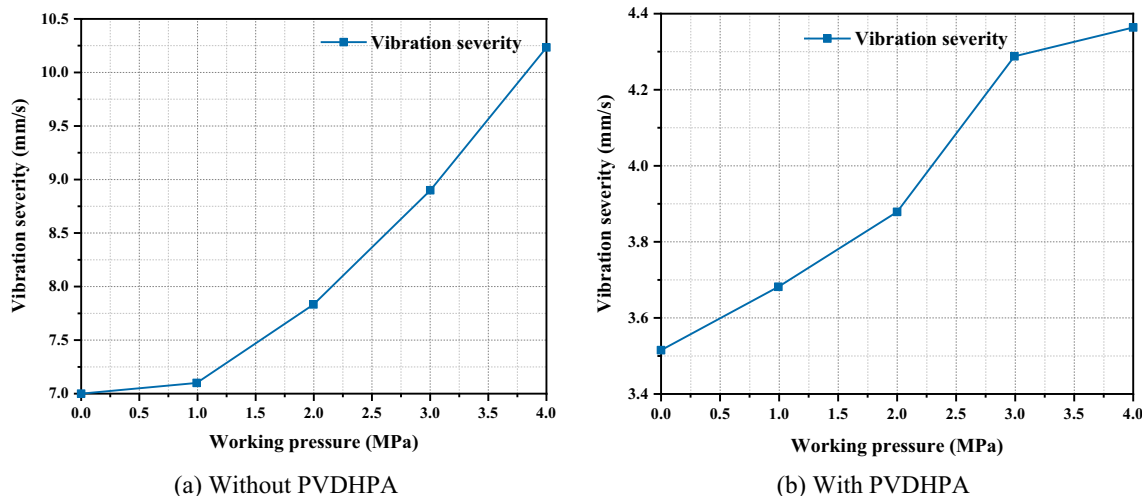
(a) Without PVDHPA

(b) With PVDHPA

Fig. 18 Fitting curve of vibration severity under different working pressures without and with the installation of PVDHPA
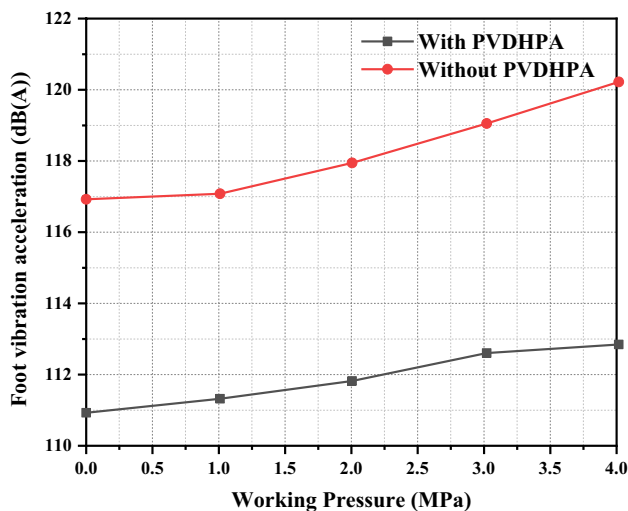

Fig. 19 Vibration acceleration of the machine foot under different working pressures without and with the installation of PVDHPA

intensities in different working conditions before and after the PVDHPA is installed.

Fitting the vibration intensity data under different working conditions listed in Table 2, the system vibration intensity before and after the PVDHPA is used as a function of working pressure is plotted in Fig. 18. After the pulsation attenuator is installed, the fitting curve function of the vibration intensity with the working pressure can be described as:

$$y = 0.2265x + 3.494 \tag{21}$$

where y is the vibration intensity, and x is the working pressure (0–4 MPa).

When the pulsation attenuator is not installed, the fitting curve function of the vibration intensity changing with the working pressure is:

$$y = 0.8255x + 6.578 \tag{22}$$

From the above test data and analysis, it can be seen that as the working pressure increases, the system vibration intensity gradually increases, and the vibration intensity values under rated conditions are 4.4 mm/s and 10.2 mm/s, respectively. When the pulsation attenuator is not installed, the vibration intensity of the direct-drive pump system increases more rapidly with the increase in working pressure. After installing the PVDHPA, the vibration intensity under the rated working condition is reduced by 57.3% compared with the non-installation. The machine foot vibration acceleration index is used as the evaluation standard and reference for the vibration performance of the direct-drive pump system. When the vibration intensity is expressed in decibels, mm/s is selected as the benchmark reference value; that is, the effective value of the vibration velocity of the reference benchmark is zero decibels. Then, the definition expression of the vibration acceleration of the machine foot is:

$$V_j = 20 \lg \frac{V_s}{V_0} \tag{23}$$

where V_j is the conversion value of machine foot vibration acceleration, V_s is the vibration intensity measurement and calculation value, V_0 is the vibration intensity reference value, and $V_0 = 10^{-5}$ mm/s.

Figure 19 illustrates the vibration acceleration of the machine foot under different working pressures, which was calculated by Eqs. (21) to (23). It can be seen from Fig. 19 that

under rated conditions, the vibration acceleration values of the machine feet before and after the installation of the PVDHPA are 120.2 dB(A) and 112.8 dB(A), respectively, which has realized the reduction of 7.4 dB(A). The test results show that the use of the PVDHPA to absorb the fluid excitation signal in the resonance frequency band of the main components of the system can effectively suppress the vibration impact and has a significant effect on reducing the vibration acceleration index of the machine foot.

5 Conclusions

The working principle, structural optimization design, and performance test of the PVDHPA are introduced in this paper. Several conclusions are drawn as follows.

1. Appropriately increasing the length of the damping hole, reducing the diameter of the damping hole, and increasing the volume of the resonant cavity within the allowable range of the overall structure will achieve a relatively good vibration absorbing effect and improve the Helmholtz pulsation attenuator ability to absorb the excitation energy in the fluid. Combined with the main resonance frequency bands of the direct-drive pump system obtained from the structural dynamics analysis, the optimized structure parameters of the porous, variable-diameter Helmholtz pipeline pulsation attenuator suitable for the large-flow direct-drive pump system are selected as follows: The length of the damping hole is 6.5 mm; the maximum diameter of the resonance cavity is 110 mm; and the damping hole diameter ranges from 2 to 4 mm.

2. After the Helmholtz pulsation attenuator is installed, the vibration response amplitude of the direct-drive pump is significantly reduced, and the vibration signal in the frequency bands around 200–400 Hz and 1000 Hz is significantly suppressed, and the vibration shock in the vertical direction is most obviously weakened. Before and after the installation of the multi-hole reducing Helmholtz pulsation attenuator, the vibration acceleration values of the machine feet under rated conditions were 120.2 dB(A) and 112.8 dB(A), respectively, a decrease of 7.4 dB(A). It shows that the porous, variable-diameter Helmholtz pulsation attenuator designed according to the conclusions of the dynamic characteristics analysis has a good damping effect on the direct-drive pump system.

Through the analysis of the above conclusions, it can be found that the structural parameters of PVDHPA have an important influence on the vibration response amplitude of the direct-drive pump. Therefore, in the future work, we will use the orthogonal experimental design and the response surface method to optimize the PVDHPA structural parameters. In addition, the proposed PVDHPA can effectively control the medium and high-frequency vibration of a direct-drive pump, but it is difficult for this device to effectively control the low-frequency vibration of a direct-drive pump, so this can be the subject of further studies.

Author contributions FG contributed to data curation, validation, and writing—original draft. SN was involved in conceptualization, project administration, and writing—review and editing. YH contributed to formal analysis, investigation, and writing—review and editing. FY was involved in investigation, methodology, and writing—review and editing. RH contributed to investigation and provided software. HJ was involved in data curation; methodology; and formal analysis.

References

1. Fagnant CS, Toles M, Zhou NA et al (2017) Development of an elution device for Viro Cap virus filters. Environ Monit Assess. https://doi.org/10.1007/s10661-017-6258-y
2. Yamasaki S, Wang L, Hirata T et al (2015) Multidrug efflux pumps contribute to Escherichia coli biofilm maintenance. Int J Antimicrob Agents 45(4):439–441. https://doi.org/10.1016/j.ijantimicag.2014.12.005
3. Chao Q, Zhang JH, Xu B et al (2022) Integrated slipper retainer mechanism to eliminate slipper wear in high-speed axial piston pumps. Front Mech Eng 17(1):1. https://doi.org/10.1007/s11465-021-0657-z
4. Ye SG, Zhang JH, Xu B et al (2018) A theoretical dynamic model to study the vibration response characteristics of an axial piston pump. Mech Syst Signal Process 150:107237. https://doi.org/10.1016/j.ymssp.2020.107237
5. Kim T, Ivantysynova M (2017) Active vibration control of swash plate-type axial piston machines with two-weight notch least mean square/filtered-x least mean square (LMS/FXLMS) filters. Energies 10(12):645. https://doi.org/10.3390/en10050645
6. Choi J, Choi Y, Kim C et al (2010) Flow uniformity in a multi-intake pump sump model. J Mech Sci Technol 24(7):1389–1400. https://doi.org/10.1007/s12206-010-0413-5
7. Birajdar R, Keste A (2020) Prediction of flow-induced vibrations due to impeller hydraulic unbalance in vertical turbine pumps using one-way fluid−structure interaction. J Vib Eng Technol 8(3):417–430. https://doi.org/10.1007/s42417-019-00174-5
8. Zhang TX (2016) The analysis of vibration characteristics for a hydraulic structural component. J Vib Eng Technol 4(6):563–571
9. Yu JF, Shou QY, Jin WL et al (2017) Evaluation of the hydraulic resonance in turbine mode of a medium-head pump-turbine. J Vib Eng Technol 5(5):451–466
10. Shang YX, Tang H, Sun HW et al (2019) A novel hydraulic pulsation reduction component based on discharge and suction self-oscillation: principle, design and experiment. Proc Inst Mech Eng

Part I J Syst Control Eng 234(4):433–445. https://doi.org/10.1177/09596651819871775

11. Edge KA, Johnston DN, Cao YB (1991) Using the second source method to measure the pressure pulsation characteristics of hydraulic pumps-test results. Mach Tool Hydraul 5:37–42. https://doi.org/10.1155/2018/2784079

12. Song YC, Xu B, Yang HY et al (2014) Design on estimation algorithm of the pump source impedance and the signal processing software for secondary source method. J Mech Eng 20:167–174. https://doi.org/10.1016/j.ijepes.2017.07.013

13. Song YC, Xu B, Yang HY et al (2014) Modified practical approximate method for testing source flow of piston pump. J Zhejiang Univ (Eng Sci) 02:200–205. https://doi.org/10.3785/j.issn.1008-973X.2014.02.003

14. Xu B, Zhang J, Yang HY et al (2013) Investigation on the radial micro-motion about piston of axial piston pump. Chin J Mech Eng 2:325–333. https://doi.org/10.3901/CJME.2013.02.325

15. Xu B, Song Y, Yang HY (2013) Pre-compression volume on flow ripple reduction of a piston pump. Chin J Mech Eng 6:1259–1266. https://doi.org/10.3901/CJME.2013.06.1259

16. Manring ND (2000) The discharge flow ripple of an axial-piston swash-plate type hydrostatic pump. J Dyn Syst Meas Control Trans ASME 2(122):263–268. https://doi.org/10.1115/1.482452

17. Zeng XR, Li XN (1988) Optimal design of cylinder block of swashplate axial piston pump. J Harbin Inst Technol 1:20–27. https://doi.org/10.4028/www.scientific.net/AMR.186.368

18. Mikota J (2001) A novel, compact pulsation compensator to reduce pressure pulsations in hydraulic systems. In: Proceedings of Ivanov-international conference on noise, acoustics and vibration

19. Orwig H (2005) Experimental and analytical vibration analysis systems. Int J Solids Struct 42:5821–5830. https://doi.org/10.1016/j.ijsolstr.2005.03.028

20. Ijaz M (2007) Damping of low-frequency pressure oscillation. Tampere University of Technology, Tampere

21. Ichiyanagi T, Nishiumi T (2008) Study on the insertion loss characteristics of side branch resonator in the hydraulic line. In: Proceedings of the 7th JFPS international symposium on fluid power

22. Nicholas EE, Kenneth AC (2012) Compact Helmholtz resonators for hydraulic systems. Int J Fluid Power 13(1):41–50. https://doi.org/10.1080/14399776.2012.10781045

23. Jing HQ, Zhang XN, Li YF et al (2013) Design and analysis of a new kind of hydraulic active filter. J Beijing Univ Aeronaut Astronaut 39(08):1091–1095

24. Gruber ER, Cunefare KA, Danzl PW et al (2013) Optimization of single and dual suppressors under varying load and pressure conditions. Int J Fluid Power 14(3):27–34. https://doi.org/10.1080/14399776.2013.10801411

25. Yuan M, Cao Z, Luo J et al (2018) Low frequency acoustic energy harvester based on a planar Helmholtz resonator. AIP Adv 8(8):085012. https://doi.org/10.1063/1.5042683

26. He SH, Zi YJ, Wen W (2015) Research of resonators based on elastic sheet/membrane elements for hydraulic system. J Sound Vib 355:54–65. https://doi.org/10.1016/j.jsv.2015.05.034

27. Li Y, Jiao ZX, Wu S (2013) Flow characteristics analysis and optimization design of high-frequency reciprocation pump applying check valve to rectification. J Mech Eng 14:154–163. https://doi.org/10.3901/JME.2013.14.154

28. Kamgar R, Tavakoli R, Rahgozar P et al (2021) Application of discrete wavelet transform in seismic nonlinear analysis of soil–structure interaction problems. Earthq Spectra 37(3):1980–2012. https://doi.org/10.1177/8755293020988027

29. Dadkhah M, Kamgar R, Heidarzadeh H (2020) Reducing the cost of calculations for incremental dynamic analysis of building structures using the discrete wavelet transform. J Earthq Eng. https://doi.org/10.1080/13632469.2020.1798830

30. Kamgar R, Rahgozar R (2016) A simple method for determining the response of linear dynamic systems. Asian J Civ Eng 17(6):785–801

31. Kamgar R, Dadkhah M, Naderpour H (2021) Seismic response evaluation of structures using discrete wavelet transform through linear analysis. Structures 29:863–882. https://doi.org/10.1016/j.istruc.2020.11.012

32. Rostami S, Kamgar R (2022) Insight to the Newmark implicit time integration method for solving the wave propagation problems. Iran J Sci Technol Trans Civ Eng 46:679–697. https://doi.org/10.1007/s40996-021-00599-7